$(e,2e)$ study of two-center interference effects in the ionization of N_2

L. R. Hargreaves,[1] C. Colyer,[1] M. A. Stevenson,[1] B. Lohmann,[1] O. Al-Hagan,[2] D. H. Madison,[2] and C. G. Ning[3]
[1]*ARC Centre of Excellence for Antimatter-Matter Studies, The University of Adelaide, Adelaide, South Australia 5005, Australia*
[2]*Department of Physics, Missouri University of Science and Technology, Rolla, Missouri 065409, USA*
[3]*Department of Physics and Key Laboratory of Atomic and Molecular NanoSciences of MOE, Tsinghua University, Beijing 100084, People's Republic of China*
(Received 6 October 2009; published 3 December 2009)

A number of previous studies have suggested the possibility of two-center interference effects in the single ionization of diatomic molecules such as H_2 and N_2. While interference effects have been successfully observed in the ionization of H_2, to date evidence for interference in N_2 ionization has yet to be conclusively demonstrated. This study presents triply differential cross sections for electron impact ionization of N_2, measured using the $(e,2e)$ technique. The data are probed for signatures of two-center interference effects. Evidence for interference manifesting in the cross sections is observed.

DOI: 10.1103/PhysRevA.80.062704 PACS number(s): 34.80.Gs

I. INTRODUCTION

The problem of single ionization of diatomic molecules by particle impact has received significant attention from atomic and molecular physicists in recent years, due to the possibility of observing two-center interference effects. Such interference can be considered analogous to a "Young's double-slit" type effect, with the two atomic centers (the slits) acting as localized sources of coherent electron emission. Understanding of interference phenomena is critical to any theoretical description of dual-nature quantum objects such as electrons and is therefore fundamental to a thorough understanding of collision-induced reactions.

If particle impact ionization of diatomics can indeed lead to interference effects, then an obvious question is how such effects can be observed in an experiment. The method generally employed by experimentalists has been to measure ionization cross sections (probabilities) for diatomic molecules, as a function of either the ionizing or ejected particle's momentum, and look for structures which could be interpreted as indicative of two-center effects. Several early experimental studies into this problem studied the doubly differential cross sections (DDCS) of H_2 [1–4] and D_2 [5] ionization by heavy ion (H_2) and electron (D_2) impact. Oscillatory structures in the DDCS (the probability of a collision yielding an electron with momentum $\boldsymbol{k}_e$ as a function of the incident particle momentum $\boldsymbol{k}_0$) were observed and interpreted by the authors as evidence of two-center interference. Alexander *et al.* [6] recently investigated a different type of DDCS—one in which the scattered projectile momentum k_s is determined instead of the ejected electron momentum $\boldsymbol{k}_e$ and they found that this type of DDCS was much more sensitive to two-center interference effects for proton-impact ionization of H_2.

Several studies [7–10] have also considered the possibility of observing interference effects in triply differential cross sections (TDCS), using the $(e,2e)$ technique. An $(e,2e)$ measurement requires the detection of both the ionizing and ejected electron, in time coincidence. Hence, the TDCS represents the probability of a collision yielding both an ejected electron with momentum $\boldsymbol{k}_e$ and a scattered electron with momentum $\boldsymbol{k}_s$, again as a function of $\boldsymbol{k}_0$. By the above definition the DDCS is determined by the integration of the TDCS over the momentum of one of the two final state continuum particles. Since integration often masks scattering effects, several authors [8,9] have suggested that interference effects may show stronger signatures in a TDCS than in a DDCS. Indeed, evidence of two-center effects has already been observed in $(e,2e)$ measurements of H_2 ionization [8,10], by comparing molecular and equivalent atomic TDCS.

Here, TDCS results from an $(e,2e)$ study of N_2 ionization are presented, with emphasis placed on examining the results for two-center interference. As a heavier target than H_2, with a correspondingly larger cross section, N_2 may be expected to show an even stronger signature of interference than H_2 [9]. The theoretical study of Gao *et al.* [7] supports interference effects in N_2 ionization, finding a pronounced oscillatory structure in the backward angle scattering of the coplanar symmetric energy-sharing TDCS, which was attributed by the authors to two-center effects. The experimental results of Murray *et al.* [9] also showed some limited evidence of two-center interference in the symmetric energy-sharing regime for N_2.

To look for two-center interference effects, the strategies of both previous studies have been employed here. First, the TDCS's of N_2 were measured and compared with theoretical TDCS results for the kinematically equivalent atomic nitrogen TDCS. The kinematics for these measurements were very similar to those employed by Milne-Brownlie *et al.* [8], with the energy sharing between the two outgoing electrons being highly asymmetric. The second approach employed has been to probe the TDCS in the symmetric energy-sharing regime to try and observe evidence of the oscillation predicted by Gao *et al.* [7]. As well as the additional measurements, improved theoretical calculations of the N_2 TDCS, employing the molecular three-body distorted wave (M3DW) approach, under both kinematics are presented.

II. EXPERIMENT DETAILS

The apparatus used for the present measurements has been described extensively in a prior publication [11] and so

only an overview is given here. A collimated electron beam of the desired energy was produced by a standard electron gun, comprising a tungsten filament electron emission source and a five-element, cylindrical geometry lens stack. The energy of the electron beam could be varied between 0–2000 eV, with an energy width around 0.5 eV full width half maximum. This electron beam intersected a molecular nitrogen beam formed by the effusive flow of nitrogen gas through a stainless steel capillary (diameter 0.7 mm, length 20 mm). The interaction region was thus formed by the volume overlap of the electron and gas beams. Two identical electron energy analyzers, mounted on independently rotatable turntables, collected electrons emerging from the interaction region. Electrons entering an analyzer were transported and focused, again by cylindrical geometry lenses, into a hemispherical energy selector which filtered the electrons according to their energy. Electrons with energies ranging from 2 eV up to the incident energy could be selectively detected, with a total system energy resolution of around 0.75 eV. Electrons which passed through the selector impacted on a channel electron multiplier (CEM). The output pulses from the two CEMs were registered and analyzed by standard fast timing electronics and coincidence circuitry.

Measurements in the present study were conducted using an asymmetric coplanar geometry. Under such geometry, the two outgoing electrons and the incident electron are in the same plane but the emission angle of the two outgoing electrons, each with respect to the incident, are different to one another. During a measurement, one electron energy analyzer was held at a fixed detection angle, typically between $-15°$ to $-25°$ with respect to the incident beam direction, while the other was scanned repeatedly over the accessible angular region until sufficient statistical precision was obtained in the data. The scanned analyzer could access electron emission angles between $35°-135°$ (the forward scattering angle or "binary" collision region) and $225°-285°$ (the backward scattering angle or "recoil" collision region), again with respect to the incident beam. The angular range accessible by the scanned electron energy analyzer was limited by the positions of the stationary analyzer and fixed electron gun. Data were accumulated for periods ranging between several days to one week per scan, depending on signal levels.

To measure the TDCS in the either the binary or recoil region, the stationary analyzer was positioned at either $-15°$ and $+15°$, respectively, with respect to the incident electron beam (where the negative angle denotes that the stationary analyzer is on the opposite side of the election beam to the scanned analyzer). Moving the stationary analyzer symmetrically about $0°$ then in effect changed the ejected electron detection angle from θ_e to $360°-\theta_e$, allowing the distribution of the TDCS in the binary or recoil region to be measured. This technique also allowed the relative magnitudes of the binary-to-recoil scattering to be determined, with an uncertainty of no more than 35%, by comparing the magnitude of the scattering signal between any two points in the binary and recoil region. In addition, the binary/recoil scattering ratios were crosschecked using a "mixed flow technique," which is presently being developed by the Adelaide group. The technique compares the coincident scattering signal from the test gas with that from a control gas (helium), and in principle enables the absolute magnitude of the TDCS to be determined. In this study, however, the use of the technique has been restricted to cross checking the binary/recoil ratios determined by the more conventional method outlined above and all cross sections reported are on a relative scale. In all cases both techniques yielded the same results to within their respective uncertainties. The full details of the technique will reported in a forthcoming publication.

To establish the kinematics for a given measurement, the incident and ejected electrons' energy were chosen and the scattered electron energy determined by energy conservation, i.e.,

$$E_s = E_0 - E_e - \varepsilon, \tag{1}$$

where E_0, E_s, and E_e are, respectively, the incident, scattered, and ejected electron energies and ε is the ionization potential of the orbital under study. The incident energies used in the present study were less than 150 eV, and the ejected electron energies less than 30 eV. In the case of asymmetric energy-sharing measurements, the stationary electron energy analyzer registers the faster of the two outgoing electrons, which is conventionally designated the scattered electron.

To ensure apparatus effects did not manifest in the measured cross sections, prior to each scan a test measurement using a helium target was performed under *identical* kinematics to the intended nitrogen measurement, save for an adjustment of either the incident or scattered energy to account for helium's different ionization potential. The results of the helium measurements were compared with convergent close-coupling (CCC) calculations [12], which were taken as benchmarked in this energy range [13]. In all instances the helium TDCS distribution was in excellent accord with the CCC results.

III. THEORY: MOLECULAR THREE DISTORTED WAVE APPROACH

The M3DW approximation has been presented elsewhere [14–16] so only a brief overview will be presented here. The M3DW TDCS is given by

$$\frac{d^5\sigma}{d\Omega_a d\Omega_b dE_b} = \frac{1}{(2\pi)^5}\frac{k_a k_b}{k_i}(|T_{dir}|^2 + |T_{exc}|^2 + |T_{dir} - T_{exc}|^2), \tag{2}$$

where $\vec{k}_i$ is the initial state wave vector, $\vec{k}_a$ ($\vec{k}_b$) is the wave vector for the scattered (ejected) electron and the direct and exchange amplitudes are T_{dir} and T_{exc}, respectively,

$$T_{dir} = \langle \chi_a^-(\vec{k}_a, \mathbf{r}_1)\chi_b^-(\vec{k}_b, \mathbf{r}_2)C_{scat-eject}(r_{12})|V - U_i|\phi_j^{OA}(\mathbf{r}_2)\chi_i^+(\vec{k}_i, \mathbf{r}_1)\rangle, \tag{3}$$

$$T_{exc} = \langle \chi_a^-(\vec{k}_a, \mathbf{r}_2)\chi_b^-(\vec{k}_b, \mathbf{r}_1)C_{scat-eject}(r_{12})|V - U_i|\phi_j^{OA}(\mathbf{r}_2)\chi_i^+(\vec{k}_i, \mathbf{r}_1)\rangle. \tag{4}$$

In Eqs. (3) and (4), $\mathbf{r}_1$ ($\mathbf{r}_2$) is the coordinate of the incident (bound) electron, χ_i, χ_a, and χ_b are the distorted waves for

the incident, scattered, and ejected electrons, respectively, $C_{scat-eject}$ is the Coulomb interaction between the scattered projectile and ejected electron, and ϕ_j^{OA} is the orientation-averaged molecular orbital [14] for the initial bound-state wave function of the molecule generated from multicenter molecular orbitals. The molecular wave function was calculated using density-functional theory along with the standard hybrid B3LYP [17] functional by means of the ADF 2007 (Amsterdam density functional) program [18] with the TZ2P (triple zeta with two polarization functions) Slater type basis sets. The potential V is the initial state interaction between the projectile and the neutral molecule, and U_i is the initial state spherically symmetric distorting potential which is used to calculate the initial state distorted wave χ_i.

The Schrödinger equation for the incoming electron wave function is given by:

$$\left(T + U_i - \frac{k_i^2}{2}\right)\chi_i^+(\vec{k}_i, \mathbf{r}) = 0, \tag{5}$$

where T is the kinetic-energy operator and the "+" superscript on $\chi_i^+(\vec{k}_i, \mathbf{r})$ indicates outgoing wave boundary conditions. The initial state distorting potential contains three components $U_i = U_S + U_E + U_{CP}$, where U_S is the initial state spherically symmetric static potential. The static potential is composed of an electronic part and a nuclear part. The electronic part is calculated from the molecular charge density obtained from the numerical orbitals averaged over all angular orientation. The nuclear part is obtained by averaging the two N_2 nuclei over all orientations (the spherical averaging of the two nuclei places a charge of +14 uniformly distributed on a sphere of radius $1.07a_0$). The exchange-distortion potential U_E is that of Furness and McCarthy (corrected for sign errors) [19] and U_{CP} is the correlation-polarization potential of Perdew and Zunger [20] (see also Padial and Norcross [21]).

The two final channel distorted waves are obtained from a Schrödinger equation similar to Eq. (5):

$$\left(T + U_f - \frac{k_{a(b)}^2}{2}\right)\chi_{a(b)}^-(\vec{k}_{a(b)}, \mathbf{r}) = 0. \tag{6}$$

Here $U_f = U_I + U_E + U_{CP}$ where U_I is the final state spherically symmetric static distorting potential for the molecular ion which is calculated using the same procedure as U_S except that the active electron is removed from the charge distribution.

The present M3DW model is an improvement over previously published M3DW results for N_2 [9]. In the earlier results, a very simple N_2 wave function and a crude polarization potential with a cut-off parameter were employed. Here, the polarization potential with a cut-off parameter has been eliminated and replaced with the Perdew-Zunger correlation-polarization potential and improved N_2 orbital calculations have been used.

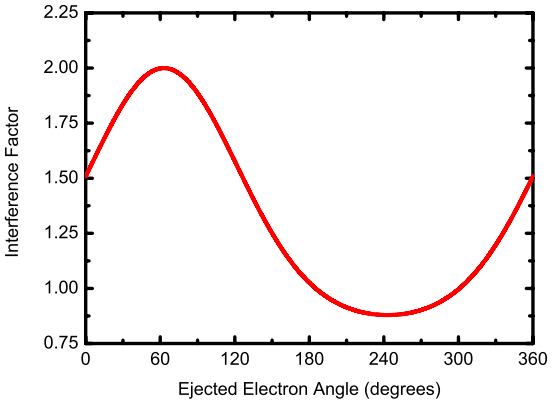

FIG. 1. (Color online) Interference factor as a function of ejected electron emission angle, for continuum-electron energies of $E_0 = 150$ eV, $E_s = 124.4$ eV, and $E_e = 10$ eV.

IV. RESULTS AND DISCUSSION

A. Asymmetric energy sharing

Under an asymmetric scattering geometry, the TDCS can be viewed as containing two distinct scattering regions. The TDCS in the binary region, located between ejected electron angles of 0° and 180°, describes the direct "knock out" of a bound electron by the incident electron. The recoil region TDCS, corresponding to ejected electron angles between 180° and 360°, arises due to a secondary, elastic collision between the ejected electron and the target nucleus. The relationship between the TDCS in the binary and recoil regions is an important consideration when considering signatures of two-center interference.

Here, the approach of Milne-Brownlie *et al.* [8] and Staicu Casagrande *et al.* [10] has been employed. Both studies were based on the work of Stia *et al.* [22], who showed that the TDCS for H_2 ionization could be approximated as:

$$\mathrm{TDCS}_{H_2} = 2I \times \mathrm{TDCS}_{H}, \tag{7}$$

where I is the "interference factor," which describes the two-center interference. The interference factor is given by:

$$I = 1 + \frac{\sin(|\boldsymbol{\chi}||\boldsymbol{\rho}_0|)}{|\boldsymbol{\chi}||\boldsymbol{\rho}_0|}, \tag{8}$$

where ρ_0 is the equilibrium internuclear separation, 1.07 Å for N_2, and $\boldsymbol{\chi}$ is:

$$\boldsymbol{\chi} = \boldsymbol{k}_s - \boldsymbol{k}_e - \boldsymbol{k}_0. \tag{9}$$

Milne-Brownlie *et al.* and Staicu Casagrande *et al.* compared the measured TDCS for H_2 with theoretical calculations of the TDCS for H, H_2, and He, and with experimental measurements of the TDCS for He, and concluded that there was evidence for interference in the cross section for H_2, based on the predictions of Eq. (7).

When plotted as a function of the ejected electron emission angle (Fig. 1), the interference factor shows a two-fold enhancement of the TDCS in the binary collision region. That is, one would expect that the binary peak for N_2 ionization is four times bigger than the equivalent atomic cross

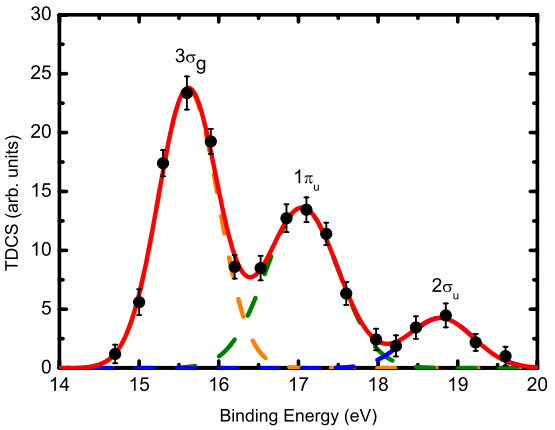

FIG. 2. (Color online) Binding energy spectrum for N_2. The three outermost orbitals (labeled in the figure) are all resolved at the current coincidence energy resolution of 850 meV.

section, rather than simply twice as big due to the additional scattering center. However, as the measured cross sections are not on an absolute scale, an increase in the binary peak due to interference could not be verified by this method. However, while the interference factor enhances the TDCS in the binary region, its effect in the recoil region is to suppress the TDCS somewhat (by a factor of 0.8). Hence, by measuring the TDCS and comparing the magnitudes of the binary and recoil scattering, two-center interference effects should manifest as a suppression of the recoil peak, relative to the binary, when compared with the atomic binary-to-recoil ratio. Note that while Stia *et al.* derived this approximation only for the case of H_2, one might expect that a similar analysis would hold, at least qualitatively, in the case of N_2 ionization.

TDCS measurements were made for ionization of the three outermost orbitals of N_2, the $3\sigma_g$, $1\pi_u$, and $2\sigma_u$ orbitals, all of which were resolved with the present coincidence energy resolution (Fig. 2). The incident electron energy was set at 150 eV and the ejected electron energy 10 eV. The measured results for each orbital are presented in Fig. 3, together with a calculated, kinematically equivalent, *atomic* nitrogen TDCS, and the same atomic TDCS multiplied by the interference factor. All three data sets have been normalized together at the binary maximum. The atomic TDCS have been calculated using the distorted-wave Born approximation (DWBA) code of McCarthy [23].

In Fig. 3, the experimental data for the three molecular orbitals are compared with the DWBA calculations for the atomic orbitals with the most similar momentum distribution. The two *u*-type molecular orbitals have been compared to the TDCS for an atomic $2p$-orbital, due to the presence of a node in both orbital momentum distributions (in fact, the $2\sigma_u$ orbital is actually an *s*-orbital hybrid). Similarly the experimental results for the $3\sigma_g$ molecular orbital, a *p*-orbital hybrid, have been plotted against an atomic $2s$-orbital calculation since both these orbitals' momentum distributions do not contain a node. Also note that the molecular continuum-electron energies were used when calculating the atomic cross sections. In effect this means that the atomic orbitals were prescribed the same ionization potential as the molecular nitrogen orbitals, rather than their physical ionization potential. This approach ensured the experimental and theoretical results were kinematically identical.

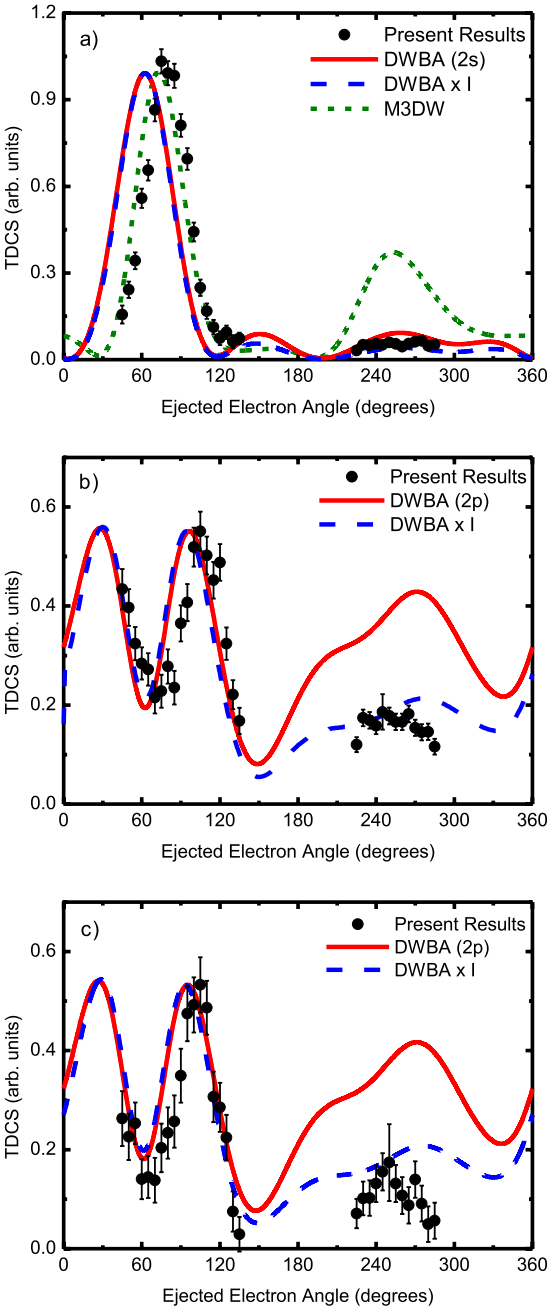

FIG. 3. (Color online) TDCS for ionization of the (a) $3\sigma_g$, (b) $1\pi_u$, and (c) $2\sigma_u$ orbitals of N_2. The incident electron energy was 150 eV, the ejected electron energy was 10 eV and the scattered electron angle −15°. The experimental results (circles) are compared with DWBA calculations for the atomic nitrogen $2s$ (a) and $2p$ (b), (c) orbitals (solid curve), and the same calculation multiplied by the interference factor (long dashed curve). Also shown is the M3DW calculation for ionization of the $3\sigma_g$ orbital of N_2 (short dashed curve).

As discussed, multiplying the atomic calculations by the interference factor decreases the magnitude of the cross section in the recoil region, relative to the binary region. Across

all three orbitals considered, the modification of the atomic calculation by the interference factor significantly improves the description of the experimental data, compared to the unmodified calculation. Indeed, the $1\pi_u$ and $2\sigma_u$ experimental results are in overall excellent agreement with the modified atomic calculations, in both the binary and recoil regions. The $3\sigma_g$ data show slightly less good agreement, with the location of the binary peak in the molecular cross section shifted with respect to the atomic calculation. Nonetheless, the binary/recoil ratio is certainly better described by the modified DWBA calculation than the straight atomic calculation. As discussed, this behavior is consistent with the influence of two-center interference on the TDCS, and hence all three data sets can be interpreted as showing evidence of interference effects.

In addition to the DWBA results, results from an M3DW calculation for *molecular* nitrogen are included in Fig. 1(a) for the $3\sigma_g$ orbital. The M3DW approach inherently incorporates two-center interference due to the two-center distorting potentials and wave functions employed in the calculations. The M3DW result is in significantly better agreement with the experimental data in terms of the position and width of the binary peak, but predicts a stronger recoil peak than is observed in the experimental data and in terms of the binary/recoil ratio, is in poorer agreement with the experiment than either of the modified or unmodified atomic calculations. In light of the good accord between the M3DW and experimental data for H_2 [8] in the recoil region, under very similar kinematics, the disparity observed here is somewhat surprising and not fully understood at this time.

B. Symmetric energy sharing

TDCS measurements were made for the $3\sigma_g$ orbital of N_2 (Fig. 4) using an incident energy of 75.6 eV and equal scattered and ejected energies of 30 eV. Measurements were made at two different scattered electron angles, −25° and −10°. The measurements at a scattering angle of −25° essentially repeat the kinematics considered in Murray *et al.* [9], while the data at −10° probe the kinematics considered in the theoretical study of Gao *et al.* [7]. In addition to the measurements, M3DW calculations at both scattered electron angles are presented.

The −25° kinematics was previously considered, both experimentally and theoretically, by Murray *et al.* [9,24]. The earlier theoretical data employed an older M3DW approach using an elementary N_2 wave function and a polarization potential with a cut-off parameter. The earlier M3DW results showed a large peak in the cross section, centered on 110°, in addition to the normal binary and recoil structures. This peak was presented as possible evidence of two-center interference, as the same approach predicted no evidence of a similar structure in the atomic TDCS under equivalent kinematics [7]. The experimental results showed a slight increase in the TDCS in the backward scattering region which was interpreted by the authors as *possible* evidence for the interference structure. However, the location of the peak was significantly shifted and much smaller in magnitude than that predicted by the theory and overall the agreement between

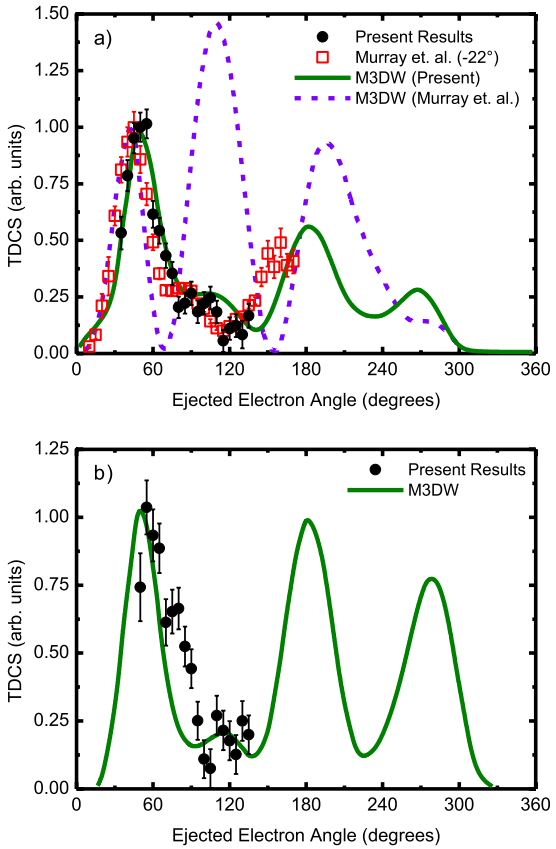

FIG. 4. (Color online) TDCS for ionization of the $3\sigma_g$ orbital of N_2. The incident electron energy was 75 eV, the scattered and ejected electron energies 30 eV, with scattered electron angles of (a) −25° and (b) −10°. The present experimental results (circles) are compared to results from M3DW calculations (solid curve), as well as results from a previous experiment (open squares) [9] and a previously published M3DW calculation (short dashed curve) [24].

the experimental and theoretical data was poor. In view of the significant discrepancy in the previous results, this kinematic regime has been further explored here.

The present results at $\theta_s = -25°$ are presented in Fig. 4(a), together with the data of Murray *et al.* [9,24] and results from the present improved M3DW calculation. Clearly, the two experimental results and the theoretical data are all in excellent accord, apart from a slight shift in the location of the binary peak. This apparent shift is a result of the slightly different scattering angle considered by Murray *et al.* ($\theta_s = -22°$). The improved M3DW calculation also retains the three peaks seen in the earlier calculation: a binary peak at 50°, recoil peak at 270° and "interference" peak at 180°. The magnitude of the interference peak is significantly reduced in the calculation, which overall is in excellent agreement with both sets of experimental results. Unfortunately, the 180° peak lies outside of the angular range of the experimental apparatus in its current configuration, and so the present experimental results do not offer any insights into this feature.

The experimental results at a scattering angle of $\theta_s = -10°$ [Fig. 4(b)] are also in generally good agreement with the M3DW calculation. In this instance, there is a small discrepancy in the location of the binary peak, with the calcu-

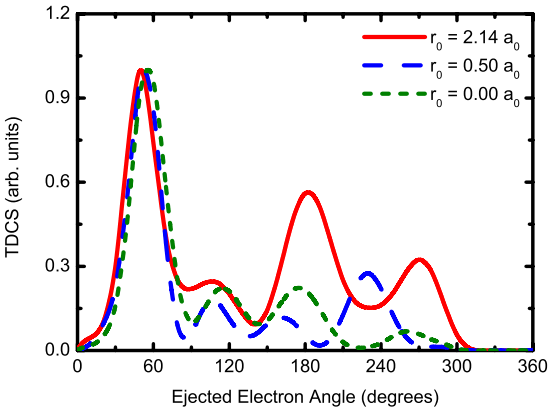

FIG. 5. (Color online) TDCS for coplanar symmetric ionization of the $3\sigma_g$ orbital of N_2. The incident energy was 75 eV, both outgoing electrons have 30 eV energy and the scattered electron angle was −22°. The M3DW calculations are for different nuclear separations r_0: $r_0=2.14a_0$ (solid curve); $r_0=0.5a_0$ (long dashed curve); and $r_0=0.0a_0$ (short dashed curve).

lation locating this peak at too small an ejection angle by around 5°. An interference peak is again predicted in the vicinity of 180° and with a somewhat stronger intensity than in the $\theta_s=-25°$ TDCS, relative to the binary peak. Again, the peak lies outside of the accessible range of the apparatus.

Gao *et al.* [7] interpreted the peak at 180° as a double-slit interference pattern resulting from electrons backscattering from two separated N_2 nuclei. Since this simple classical picture would suggest that the 180° peak is determined solely by the nuclear separation and not the electronic distribution, the dependence of the cross section on the nuclear separation was examined for a fixed electronic distribution. In Fig. 5, M3DW results for the TDCS at a scattering angle of −22° (normalized together at the binary maximum) are presented where the size of the nuclear separation is reduced from $2.14a_0$ to a point charge while keeping everything else unchanged. If the 180° peak is due to backscattering from two separate nuclei, the peak should reduce in magnitude as the nuclei are brought closer together and disappear completely when the distance between the nuclei is reduced to a point charge [25]. However, as is clear from Fig. 5, the results do not bear out such behavior. The peak persists even when the nuclear separation reduces to a point charge and the magnitude minimizes at $0.5a_0$, before increasing again with further reduction in nuclear separation. Therefore, the present results do not support the original suggestion of Gao *et al.* [7] that the 180° peak is a Young-type interference resulting from nuclear scattering. On the other hand, it certainly represents interference of some type between amplitudes and is supported by the existing experimental data.

V. CONCLUSIONS

TDCS data for ionization of N_2 molecules have been presented and examined for signatures of two-center interference effects. The current data consider two different approaches for detecting two-center interference. For higher energies and asymmetric kinematics, the molecular recoil peak is suppressed compared to theoretical atomic recoil peaks in accordance with the two-center predictions. For lower-energy symmetric collisions, the present results are in very good agreement with previous experimental measurements and the improved M3DW results. The M3DW predicts a peak at 180° scattering which had previously been interpreted as a double scattering interference peak. Although this angular range is not accessible to the present measurements, the 180° peak is consistent with earlier measurements. However, model calculations with different nuclear separations suggest that this peak does not result from electron scattering from two separate nuclei. Consequently, the present results suggest that two-center effects can be seen in the ratio of recoil peak to binary peak but that other peak structures predicted by the theory are probably due to some other type of interference which is yet to be determined.

ACKNOWLEDGMENTS

This work was supported by the Australian Research Council under a Centre of Excellence Scheme and the American NSF under Grant No. 0757749. C.G.N. would like to acknowledge the support of the National Natural Science Foundation of China under contract No. 10704046 and O.A.-H. would like to acknowledge the support of the Saudi Ministry of Higher Education's King Abdullah Bin Abdul-Aziz Scholarship.

[1] N. Stolterfoht *et al.*, Phys. Rev. Lett. **87**, 023201 (2001).
[2] N. Stolterfoht, B. Sulik, B. Skogvall, J. Y. Chesnel, F. Fremont, D. Hennecart, A. Cassimi, L. Adoui, S. Hossain, and J. A. Tanis, Phys. Rev. A **69**, 012701 (2004).
[3] D. Misra, U. Kadhane, Y. P. Singh, L. C. Tribedi, P. D. Fainstein, and P. Richard, Phys. Rev. Lett. **92**, 153201 (2004).
[4] D. Akoury *et al.*, Science **318**, 949 (2007); N. Stolterfoht *et al.*, Phys. Rev. A **67**, 030702(R) (2003); D. Misra, A. Kelkar, U. Kadhane, A. Kumar, L. C. Tribedi, and P. D. Fainstein, *ibid.* **74**, 060701(R) (2006).
[5] O. Kamalou, J.-Y. Chesnel, D. Martina, F. Fremont, J. Hanssen, C. R. Stia, O. A. Fojon, and R. D. Rivarola, Phys. Rev. A **71**, 010702(R) (2005).
[6] J. S. Alexander, A. C. Laforge, A. Hasan, Z. S. Machavariani, M. F. Ciappina, R. D. Rivarola, D. H. Madison and M. Schulz, Phys. Rev. A **78**, 060701(R) (2008).
[7] J. Gao, D. H. Madison, and J. L. Peacher, Phys. Rev. A **72**, 032721 (2005).
[8] D. S. Milne-Brownlie, M. Foster, J. Gao, B. Lohmann, and D. H. Madison, Phys. Rev. Lett. **96**, 233201 (2006).
[9] A. J. Murray, M. J. Hussey, J. Gao, and D. H. Madison, J. Phys. B **39**, 3945 (2006).
[10] E. M. Staicu Casagrande, A. Naja, A. Lahmam-Bennani, A. S. Kheifets, D. H. Madison, and B. Joulakian, J. Phys.: Conf. Ser.

141, 012016 (2008).
[11] M. A. Haynes and B. Lohmann, J. Phys. B **33**, 4711 (2000).
[12] I. Bray (private communication).
[13] M. Dürr, C. Dimopoulou, B. Najjari, A. Dorn, and J. Ullrich, Phys. Rev. Lett. **96**, 243202 (2006).
[14] J. Gao, J. L. Peacher, and D. H. Madison, J. Chem. Phys. **123**, 204302 (2005).
[15] J. Gao, D. H. Madison, and J. L. Peacher, J. Chem. Phys. **123**, 204314 (2005).
[16] J. Gao, D. H. Madison, and J. L. Peacher, J. Phys. B **39**, 1275 (2006).
[17] C. Lee, W. Yang, and R. G. Parr, Phys. Rev. B **37**, 785 (1988).
[18] C. F. Guerra *et al.*, Theor. Chim. Acta **99**, 391 (1998).
[19] J. B. Furness and I. E. McCarthy, J. Phys. B **6**, 2280 (1973).
[20] J. P. Perdew and A. Zunger, Phys. Rev. B **23**, 5048 (1981).
[21] N. T. Padial and D. W. Norcross, Phys. Rev. A **29**, 1742 (1984).
[22] C. R. Stia, O. A. Fojon, P. F. Weck, J. Hanssen, and R. D. Rivarola, J. Phys. B **36**, L257 (2003).
[23] I. E. McCarthy, Aust. J. Phys. **48**, 1 (1989).
[24] A. J. Murray, M. J. Hussey, C. Kaiser, J. Gao, and D. H. Madison, J. Electron Spectrosc. Relat. Phenom. **161**, 11 (2007).
[25] O. Al-Hagan, C. Kaiser, D. Madison, and A. J. Murray, Nat. Phys. **5**, 59 (2009).